THE ASTROPHYSICAL JOURNAL, 444:97–112, 1995 May 1

SPECTROSCOPY OF LUMINOUS INFRARED GALAXIES AT 2 MICRONS. I. THE ULTRALUMINOUS GALAXIES ($L_{IR} \gtrsim 10^{12}\ L_\odot$)

JEFFREY D. GOLDADER[1] AND R. D. JOSEPH[1]
Institute for Astronomy, University of Hawaii, 2680 Woodlawn Drive, Honolulu, HI 96822;
goldader@galileo.ifa.hawaii.edu, joseph@hubble.ifa.hawaii.edu

RENÉ DOYON[1]
Départment de Physique, Université de Montréal, C.P. 6128, Succ. A., Montréal, Quebec, Canada H3C 3J7;
doyon@astro.umontreal.ca

AND

D. B. SANDERS[1]
Institute for Astronomy, University of Hawaii, 2680 Woodlawn Drive, Honolulu, HI 96822;
sanders@galileo.ifa.hawaii.edu

Received 1993 May 13; accepted 1994 November 2

ABSTRACT

We present high-quality spectra covering the K window at a resolving power of 340 for a sample of 13 ultraluminous ($L_{IR} \gtrsim 10^{12}\ L_\odot$) infrared-selected galaxies, and line fluxes for a comparison sample of 24 lower luminosity galaxies. The 2 μm spectra of 10 of the ultraluminous galaxies are characterized by emission and absorption features commonly associated with stars and star formation; two others have the red power-law spectra and Brγ line widths of Seyfert 1 galaxies; the final galaxy has strong emission from hot dust. We have found no broad-line active nuclei not already known from optical observations, despite the fact that the extinction at 2 μm is 1/10 that at optical wavelengths; any putative Seyfert 1 nuclei must be deeply buried.

Powerful continua and emission lines from H_2 and Brγ are detected in all the ultraluminous galaxies. Comparing the H_2 1–0 $S(1)$, Brγ, and 2 μm and far-infrared luminosities to those of the lower luminosity galaxies yields several major results. First, the dereddened Brγ emission, relative to the far-infrared luminosity, is significantly depressed in the ultraluminous sample, when compared to the lower luminosity galaxies. Five of the ultraluminous galaxies have $L_{Br\gamma}/L_{IR}$ ratios lower than for any of the comparison objects. Second, the H_2 1–0 $S(1)$ luminosity is proportional to the far-infrared luminosity, This suggests that the process producing the far-infrared luminosity is also responsible, directly or indirectly, for producing the excited H_2, and that the H_2 apparently comes from optically thin regions in both classes of objects. Third, eight of the 13 ultraluminous systems have lower 2 μm/far-infrared luminosity ratios than any of the lower luminosity galaxies, and five of these are the galaxies also deficient in Brγ. These three findings may be understood if the H_2, Brγ, and 2 μm continua in the ultraluminous galaxies arise from spatially distinct regions, with the continuum and Brγ largely coming from volumes optically thick even at 2 μm, and obscured in such a fashion that the extinctions measured using optical spectroscopy do not properly measure the true optical depths. If this is the case, then even near-infrared spectroscopy may be unable to exclude the presence of undetected powerful active galactic nuclei in the ultraluminous galaxies.

Subject headings: galaxies: active —galaxies: starburst — infrared: galaxies

1. INTRODUCTION

The first large-scale survey of the sky at mid- and far-infrared wavelengths was conducted by the *Infrared Astronomical Satellite* (*IRAS*). One of the surprises to emerge from the *IRAS* survey was the discovery of a significant population of ultraluminous infrared bright galaxies ($L_{IR} \geq 10^{12}\ L_\odot$) (ULIBGs)[2] with space densities exceeding those of optically selected QSOs with comparable bolometric luminosities. Among the fundamental questions raised by this discovery is whether a burst of star formation or a buried active galactic nucleus (AGN) is the underlying energy source (e.g., Joseph & Wright 1985; Sanders et al. 1988a). Another is the origin of the very powerful H_2 quadrupole emission discovered in some of these galaxies (e.g., Joseph, Wright, & Wade 1984) and the diagnostic information it might provide in understanding the most powerful "infrared" galaxies.

One of the most useful samples for detailed studies of infrared luminous galaxies is the flux-limited *IRAS* Bright Galaxy Sample (BGS) identified by Soifer et al. (1987) and its extension to southern declinations and low Galactic latitudes by Sanders et al. (1994). We are currently embarked on a major infrared spectroscopic study of a complete sample of the luminous galaxies in the BGS, objects with $L_{IR} \geq 10^{11.2}\ L_\odot$ (LIBGs), observable from the United Kingdom Infrared Telescope (UKIRT) on Mauna Kea. Our primary motivation is to address some of the basic questions mentioned above: what are the ultimate power sources; are there obscured active nuclei in these systems; what excites the luminous H_2 emission seen in some systems; are the optical depths high at near-infrared wavelengths?

During our initial observations, highest priority was placed on obtaining data for the most luminous objects in our sample.

[1] Visiting Astronomer at the United Kingdom Infrared Telescope, which is operated by the Royal Observatories on behalf of the United Kingdom Particle Physics and Astronomy Research Council.

[2] $L_{IR} \equiv L(8\text{–}1000\ \mu\text{m})$, assuming $H_0 = 75$ km s^{-1} Mpc^{-1} and $q_0 = 0$ (see Perault 1987).

We observed eight of the 10 ULIBGs from the original BGS that were visible from UKIRT, excluding the two with the faintest 60 μm flux, and five of the eight ULIBGs from the extension to the BSG that were visible from UKIRT (the three unobserved galaxies from the extension list were identified only after we completed the observations for this paper and are also at the faint end of the sample). Thus, our observations represent 72% (13/18) of the ULIBGs visible from UKIRT, and the results should represent a fairly complete and unbiased study of the properties of these objects. All of our ULIBG spectra are presented in this paper, along with tables of measured line and continuum properties. In addition to the ULIBG observations, we were able to obtain spectra for 24 lower luminosity LIBGs, representing approximately 30% of the total number of objects in the range $L_{IR} = 10^{11.2-11.96}$. We give line powers and continuum measurements for these objects in this paper, primarily in order to have a proper comparison sample of lower luminosity objects for reasons described below. We are in the process of completing observations of a larger sample of the lower luminosity objects and will present all of the spectra, along with a full statistical analysis of the line and continuum properties of the lower luminosity LIBGs in Goldader et al. (1995; hereafter Paper II).

The current study has two principal advantages over previous work. First, improvements in detectors and instruments allow us to obtain high signal-to-noise measurements on even faint galaxies in a relatively short amount of integration time. Second, although some spectroscopic measurements of luminous infrared galaxies exist in the literature, most of the spectra were obtained with many different instruments and analyzed in a variety of ways. In contrast, our sample was obtained with only two configurations of the same instrument and analyzed homogeneously.

2. OBSERVATIONS AND DATA REDUCTION

Table 1 lists the basic properties of the galaxies presented in this paper. The names are in column (1); the positions in columns (2) and (3) are taken from radio data in the literature (Condon et al. 1990, 1991 [hereafter CHYT], 1994); the redshifts in column (4) and infrared luminosities in columns (6)[3] and (7) are from Soifer et al. (1987) and Sanders et al. (1994). We obtained optical spectroscopic classifications from Veilleux et al. (1994), who used line ratios to classify the galaxies as Seyfert, low-ionization nuclear emission-line region (LINER), and starburst; these are given in column (8).

The 2–2.5 μm spectra of the ULIBGs were obtained with the CGS4 spectrometer (Mountain et al. 1990) on UKIRT on the nights of 1991 September 19, 1992 April 20, 21, and 22, and 1993 March 8 UT. Integration times were generally 60–90 minutes, and sky frames were obtained in all but one case (IRAS 23365+3604) by nodding along the slit, allowing continuous observation of the galaxies. The spectra were fully sampled at a resolving power of 340 (890 km s^{-1}, $\sim$0.0034 μm per point), with a slit width and pixel size of 3″ on the sky. We generally extracted the spectra in 3 pixels along the slit; outside of these few pixels, relatively little signal, or none at all, was observed. Our slit sizes are small compared to the optical extent of some of the systems, but radio observations show that the radio emission, and consequently the far-infrared emission, is generally concentrated in the inner arcsecond of the galaxies (e.g., CHYT). Hence, we believe we are covering the regions responsible for generating the bulk of the luminosity detected by *IRAS*. Table 2 lists the apertures used, in arcseconds and projected dimension, in columns (2) and (3). Columns (4) and (5) list the power-law slope of the continuum and photometric CO index (discussed below). Absolute magnitudes derived from our spectra are given in column (6), and those magnitudes after reddening corrections (§ 3.2) are given in column (7). In order of priority, the slit was centered on the radio peak when precise coordinates were known, on the near-infrared peak when *K*-band images were available, and on the brightest optical source when no other information existed.

To properly sample the CGS4 spectrum in the configuration usually used for these measurements, four individual spectra were obtained, with the spectrum shifted by $\frac{1}{2}$ pixel over 2 pixels. (Some of the comparison sample objects were obtained with a different instrument configuration which is described below.) This has the side benefit of allowing the removal of the effects of bad pixels, except in the case of adjacent pairs of bad pixels in a single row. In practice, bad pixels had very little effect on our data, since the galaxies and stars were purposely placed in rows free of pairs of bad pixels. Furthermore, the emission from the galaxies was compact, generally concentrated in one or two rows. Basic data reduction (following the discussion in Doyon et al. 1994b, and performed using IRAF and routines written for IRAF by Doyon) consisted of the following.

1. First, each object spectrum was subtracted by the corresponding sky frame. This removes bias and dark current and partially removes the strong telluric OH emission lines.
2. All four spectra were flat-fielded using spectra taken of a blackbody calibration unit.
3. Polynomials were fitted to the OH line residuals and used to remove these residuals. The points used in the fit were chosen to exclude emission from the galaxies and stars.
4. The four spectra were normalized and then merged, forming a properly sampled, sky-subtracted, flat-fielded spectrum.
5. Since the integration times were short, at most 20 s, many integrations were necessary to obtain high signal-to-noise ratios. At this point, the spectra obtained from each set of integrations were normalized and coadded. The standard deviations of the means of the signal at each point were used to make an "error spectrum," from which errors were propagated through the remainder of the data reduction process.
6. Using spectra of argon and krypton calibration lamps, we calibrated the spectra in wavelength.
7. To correct for the atmospheric and instrumental responses, each row of the spectrum was divided by the spectrum of an early-type (spectral type F and earlier) star. The resultant image was multiplied by a blackbody at the effective temperature of the standard, to restore the intrinsic spectral shape of the galaxy. Using spectroscopic observations of flux standards, absolute calibration was obtained.

The spectroscopic standards were stars of spectral type F and earlier taken from the Bright Star Catalogue (Hoffleit 1982) and were observed generally both immediately before and after the galaxies and at nearly identical air masses. We chose early-type stars because the metal features seen in

[3] We note here that although we classify the galaxies on the basis of their total infrared luminosity, L_{IR}, we also use the far-infrared luminosity, $L_{FIR} \equiv L(40\text{–}120\ \mu m)$, computed using the prescription in Appendix B of Catalogued Galaxies and Quasars Observed in the *IRAS* Survey (1989), to maintain consistency with many earlier studies that used L_{FIR}.

TABLE 1A

ULTRALUMINOUS GALAXIES

Galaxy	RA (1950.0)	DEC	cz (km s^{-1})	D (Mpc)	$\log(L_{FIR}/L_\odot)$	$\log(L_{IR}/L_\odot)$	Class[a]
(1)	(2)	(3)	(4)	(5)	(6)	(7)	(8)
IRAS 05189 −2524	05 18 58.6	−25 24 40	12706	166	11.92	12.09	S2
IRAS 08572 +3915	08 57 13.0	39 15 40	17480	236	12.02	12.11	L
IRAS 09111 −1017[b]	09 11 11.1	−10 07 01	16205	219	11.91	11.99	...
IRAS 10565 +2448	10 56 35.5	24 48 43	12501	170	11.90	12.00	H
IRAS 12112 +0305	12 11 12.2	03 05 20	21703	292	12.20	12.26	...
Mrk 231	12 54 04.8	57 08 38	12556	173	12.36	12.53	S1
Mrk 273	13 42 51.6	56 08 13	11400	157	12.07	12.14	L
IRAS 14378 −3651	14 37 53.4	−36 51 44	20125	271	12.03	12.11	...
IRAS 15250 +3609	15 25 03.1	36 09 00	16009	219	11.89	11.97	L
Arp 220	15 32 46.3	23 40 08	5452	78	12.12	12.18	S2[d]
IRAS 17208 −0014	17 20 48.2	−00 14 17	12946	174	12.36	12.40	H
IRAS 19297 −0406	19 29 42.5	−04 06 34	25839	344	12.30	12.36	H
IRAS 23365 +3604	23 36 31.5	36 04 26	19484	258	12.05	12.14	L

TABLE 1B

COMPARISON SAMPLE GALAXIES

Galaxy	RA (1950.0)	DEC	cz (km s^{-1})	D (Mpc)	$\log(L_{FIR}/L_\odot)$	$\log(L_{IR}/L_\odot)$	Class[a]
(1)	(2)	(3)	(4)	(5)	(6)	(7)	(8)
NGC 695	01 48 28.1	22 20 10	9769	130	11.51	11.63	H
MCG+05-06-036	02 20 23.6	31 58 09	10106	133	11.46	11.57	...
NGC 1068	02 40 07.2	−00 13 30	1125	14	10.89	11.26	S2
NGC 1614	04 31 35.8	−08 40 55	4745	61	11.39	11.58	H
UGC 3094	04 32 38.3	19 04 07	7414	98	11.17	11.21	...
UGC 3608	06 53 52.7	46 28 11	6488	88	11.14	11.30	...
NGC 2342	07 06 20.5	20 43 04	5174	71	11.18	11.22	...
NGC 2388	07 25 38.2	33 55 29	4036	56	11.11	11.21	H
NGC 2623	08 35 25.2	25 55 48	5538	76	11.47	11.55	...
MCG +08-18-012	09 33 18.5	48 41 53	7790	108	11.21	11.31	H
NGC 3110	10 01 32.2	−06 14 02	4840	66	11.12	11.22	H
A1101+41	11 01 05.8	41 07 08	10350	142	11.52	11.58	...
MCG +00-29-023	11 18 38.6	−02 42 36	7230	99	11.10	11.24	H
Arp 193	13 18 19	34 23 49	6870	97	11.51	11.58	L
NGC 5256[c]	13 36 14.2	48 31 52	8285	116	11.34	11.47	L
Zw 247.020	14 17 53.8	49 27 54	7800	110	11.20	11.32	H
I Zw 107[c]	15 16 19	42 55 41	12043	166	11.72	11.85	H
NGC 6090	16 10 24	52 35 06	8733	122	11.33	11.48	H
IRAS 16164 −0706	16 16 29.5	-07 46 49	6674	92	11.28	11.41	L
MCG +01-42-088	16 28 27.4	04 11 24	7075	98	11.24	11.33	H
NGC 6240	16 50 27.7	02 28 58	7393	101	11.69	11.83	L
IRAS 17138 −1017	17 13 50.7	−10 17 29	5323	73	11.25	11.39	...[e]
NGC 7469	23 00 44.6	08 36 18	4963	66	11.41	11.59	S1
Zw 475.056	23 13 31.2	25 16 48	8215	111	11.37	11.53	S2

[a] Optical spectroscopic classifications based on line ratios from Veilleux et al. 1994 when available: H = H II region; L = LINER; S1 = Seyfert 1; S2 = Seyfert 2.

[b] Two galaxies are found at the position of IRAS 09111 − 1007; our spectrum is of the SW source nearest the *IRAS* coordinates; the NE source is 40″ distant.

[c] The spectrum was centered on the *K*-band peak.

[d] The Arp 200 classification of Veilleux et al. 1994 is tentative.

[e] DePoy et al. 1988 find no evidence for AGN activity in IRAS 17138 − 1017.

absorption in late-type stars would have masked out stellar absorption features in the galaxies or possibly created spurious emission features. These stars show atomic hydrogen absorption lines (e.g., Brγ), so we used Gaussian fits to remove these absorption features. The atmospheric transparency during observations of the ULIBGs was constant to better than 10%, except for IRAS 19297 − 0406, whose line and continuum strengths were adjusted upward by 10% in the tables to account for transparency variations apparent in the before-and-after spectra of the comparison star. We took effective temperatures from Landolt-Börnstein (1982) and $V-K$ colors from Johnson (1966). Our derived K magnitudes for the galaxies agree with values from the literature (e.g., Carico et al. 1988; Sanders et al. 1988a; Carico et al. 1990) to within about

TABLE 2

APERTURES, CONTINUUM, AND CO DATA

Galaxy	Aperture arcsec	Aperture kpc	β	CO_{ph}	M_K	M_K^{corr}
(1)	(2)	(3)	(4)	(5)	(6)	(7)
ULTRALUMINOUS GALAXIES						
IRAS 05189 −2524	3 x 9	2.5 x 7.5	0.29 ± 0.02	0.01 ± 0.01	−25.87	−26.53
IRAS 08572 +3915	3 x 9	3.5 x 10.6	3.13 ± 0.08	...	−23.69	−24.07
IRAS 09111 −1007	3 x 9	3.3 x 9.9	−1.48 ± 0.15	0.20 ± 0.04	−24.37	−24.75
IRAS 10565 +2448	3 x 9	2.6 x 7.7	−1.85 ± 0.07	[a]	−24.22	−24.79
IRAS 12112 +0305	3 x 9	4.4 x 13.1	−1.60 ± 0.15	...	−23.66	−23.76
Mrk 231	3 x 9	2.6 x 7.8	0.24 ± 0.03	0.03 ± 0.01	−27.03	−27.68
Mrk 273	3 x 15	2.4 x 11.4	−1.45 ± 0.09	0.16 ± 0.02	−24.25	−24.60
IRAS 14378 −3651	3 x 6	3.9 x 7.9	−1.49 ± 0.24	...	−23.58	−23.58
IRAS 15250 +3609	3 x 3	3.3 x 3.3	−2.36 ± 0.14	0.20 ± 0.03	−23.36	−23.61
Arp 220	3 x 15	1.2 x 5.7	−1.43 ± 0.07	0.24 ± 0.01	−22.98	−23.98
IRAS 17208 −0014	3 x 9	2.6 x 7.8	−1.84 ± 0.13	0.21 ± 0.03	−24.32	−24.93
IRAS 19297 −0406	3 x 3	5.2 x 5.2	−2.05 ± 0.10	...	−23.81	−24.32
IRAS 23365 +3604	3 x 9	3.9 x 11.6	−1.90 ± 0.21	0.06 ± 0.04	−24.11	−24.40
COMPARISON SAMPLE GALAXIES						
NGC 695	3 x 12	2.0 x 7.6	−2.19 ± 0.08	0.09 ± 0.03	−23.49	−23.82
MCG+05-06-036	3 x 9	2.0 x 6.0	−2.79 ± 0.07	0.19 ± 0.02	−24.25	−24.25
NGC 1068	4.5 x 1.5	0.3 x 0.1	2.27 ± 0.03	...	−23.36	−23.58
NGC 1614	3 x 12	0.9 x 3.5	−2.97 ± 0.06	0.12 ± 0.03	−23.32	−23.64
UGC 3094	3 x 9	1.5 x 4.4	−1.32 ± 0.09	0.15 ± 0.02	−23.32	−23.32
UGC 3608	3 x 9	1.3 x 4.0	−2.18 ± 0.17	0.16 ± 0.02	−22.17	−22.17
NGC 2342	3 x 9	1.1 x 3.2	−2.60 ± 0.08	0.16 ± 0.02	−22.11	−22.11
NGC 2388	3 x 9	0.9 x 2.5	−2.09 ± 0.05	0.21 ± 0.02	−23.47	−23.91
NGC 2623	3 x 9	1.1 x 3.4	−1.30 ± 0.07	0.23 ± 0.01	−22.98	−23.44
MCG +08-18-012	3 x 9	1.6 x 4.9	−1.75 ± 0.06	0.23 ± 0.02	−23.11	−23.48
NGC 3110	3 x 9	1.0 x 3.0	−1.94 ± 0.05	0.21 ± 0.02	−22.40	−22.69
A1101+41	3 x 9	2.1 x 6.4	−1.79 ± 0.13	0.21 ± 0.03	−23.80	−24.10
MCG +00-29-023	3 x 9	1.5 x 4.4	−1.53 ± 0.08	0.19 ± 0.01	−23.45	−23.92
Arp 193	3 x 9	1.5 x 4.4	−1.36 ± 0.08	0.18 ± 0.02	−22.89	−23.34
NGC 5256	3 x 9	1.7 x 5.2	−1.87 ± 0.07	0.16 ± 0.01	−23.34	−23.50
Zw 247.020	3 x 9	1.7 x 5.0	−1.88 ± 0.10	0.24 ± 0.02	−23.37	−23.84
I Zw 107	3 x 9	2.5 x 7.5	−1.77 ± 0.12	0.19 ± 0.03	−23.50	−24.07
NGC 6090	3 x 9	1.8 x 5.5	−2.35 ± 0.08	0.15 ± 0.04	−23.17	−23.36
IRAS 16164 −0746	3 x 9	1.4 x 4.1	−1.47 ± 0.08	...	−22.59	−23.13
MCG +01-42-088	3 x 9	1.5 x 4.4	−1.73 ± 0.11	0.19 ± 0.01	−23.03	−23.51
NGC 6240	3 x 9	1.5 x 4.6	−1.34 ± 0.14	0.21 ± 0.01	−24.40	−24.93
IRAS 17138 −1017	3 x 9	1.1 x 3.3	−1.72 ± 0.07	0.18 ± 0.02	−23.07	−23.39
NGC 7469	3 x 9	1.0 x 3.0	−0.78 ± 0.03	0.08 ± 0.01	−24.54	−24.54
Zw 475.056	4.5 x 1.5	2.5 x 0.8	−0.80 ± 0.06	...	−23.41	−23.78

[a] IRAS 10565 + 2448 has a high CO index, approximately 0.2–0.25.

20% for every galaxy with published small aperture ($\leq 5''$) photometry.

The comparison galaxy spectra were obtained with two instrument configurations. The first configuration, used for all but two of the galaxies, was the one described above. The second configuration used the long focal length camera on CGS4. As a result, the pixel and slit sizes were 1".5 on the sky. These spectra have twice the resolving power of the others, but only a single data point was taken in each resolution element (i.e., they are not double sampled). Two spectra were taken, shifted by one pixel, to remove bad pixels. Each sample covers approximately the same wavelength range as for the other spectra (~ 0.0034 μm). The galaxies affected by this are NGC 1068 and Zw 475.056. With only 1 pixel per resolution element, the instrumental resolution was about 460 km s^{-1}, but the undersampling creates an effective resolution poorer than this. Paper II will contain a more detailed discussion.

Emission-line strengths were obtained by the method discussed in § 3.3. The depths of the stellar CO bandheads at 2.3 μm were quantified by measuring the ratio of the flux from 2.30–2.34 μm (in the rest frame) to that of the nearby continuum (in the sprit of the spectroscopic CO index defined by Doyon, Joseph, & Wright 1994a) and were calibrated against the stars observed by Kleinmann & Hall (1986) to yield photometric CO indices (CO_{ph}; Frogel et al. 1978). Our CO index is linearly related to the spectroscopic and photometric CO indices, with only a small dispersion in the relation. Our CO index (which we call CO′) is transformed into the photometric

index as

$$CO_{ph} = \frac{CO' + 0.01}{1.05}, \quad (1)$$

and into the spectroscopic index as

$$CO_{sp} = 1.39 \times CO' . \quad (2)$$

Our CO indices agree well with those given by Ridgway, Wynn-Williams, & Becklin (1994) for 10 of the 11 galaxies present in both our sample and theirs; NGC 1614 is the only exception. We will discuss this in Paper II.

The errors in the CO index are difficult to quantify precisely. Doyon et al. (199a) found that the principal source of error is usually the normalization of the continuum (the parameter α in a power-law fit to the continuum of the form $F_\lambda = \alpha \times \lambda^\beta$). When α and β are fitted simultaneously, a small change in β results in a large change in α. However, for a *fixed* β, the errors in α are smaller than those returned by the simultaneous fitting procedure. To determine the actual fractional error in the continuum normalization, we examined the range of values for α that were consistent with the error bars of the data when β was fixed to the value determined by the simultaneous fit. This gives the approximate uncertainty in CO′, in magnitudes, and is recorded in Table 2. The uncertainty in β depends critically on which points are used to select the continuum. In these objects, where so many lines are present and unresolved at our resolution, this can be problematical. However, experience has shown us that typical uncertainties in β range from 0.1–0.2, with a few cases where it can be 0.3–0.4. Only when the uncertainty in β is very large will it significantly affect the accuracy of the CO measurement, and even then, the effect is usually not large.

Spectra of the ULIBGs are presented in Figure 1. Figure 2 shows the detailed fits to the Brγ and H_2 $v = 1$–0 $S(1)$ lines of the ULIBGs. Tables 2, 3, and 4 contain extracted and derived quantities for both groups of objects (the spectra of the lower luminosity systems will be presented in a future paper). The uncertainties given in the tables include only the random errors in the data and not absolute flux calibration errors; we estimate these conservatively as 15% or less.

3. ANALYSIS AND DISCUSSION

3.1. *General Features of the Spectra*

Three broad classes of spectra are present in the ULIBGs. Ten of the spectra consist of continua decreasing toward the red, which can be represented by power laws ($F_\lambda = \alpha \times \lambda^\beta$) with $\beta = -1.43$ to -2.36, upon which are superposed numerous emission and absorption features. They show deep CO absorption, with photometric CO indices of $\sim$0.16–0.24 indicating most of the light at 2 μm comes from late-type giants and supergiants. The properties of these galaxies (their continuum slopes, prominent CO features, and strong, unresolved Brγ recombination lines) are all those characteristic of starburst galaxies. Two of the remaining three galaxies have red power-law indices of approximately +0.27; they exhibit broad Brγ, and their very low CO indices of 0.01 and 0.03 indicate that little of the light at 2.2 μm comes from late-type stars. These are the two optical Seyfert galaxies IRAS 05189−2524 and Mrk 231; their 2 μm spectra appear to be dominated by characteristics expected of AGNs. The final galaxy is IRAS 08572+3915, which is uniquely red among the ULIBGs (Sanders et al. 1988a) and has a power-law index of +3.13. This is consistent with Carico et al.'s (1988) suggestion that a substantial fraction of the 2 μm emission of this object is due to hot ($\sim$500 K) dust. We note that IRAS 05189−2524, IRAS 08572+3915, and Mrk 231 are the three objects in this paper that are also members of the "warm" color-selected sample that are considered to be transition objects between the ULIBGs and optically selected QSOs (Sanders et al. 1988b).

Table 3 lists directly measured line strengths and widths. The Brγ fluxes and errors are given in column (2), the dispersions of the best-fit Gaussian in column (3), and the same quantities for the 1–0 $S(1)$ line in columns (4) and (5) (see § 3.3, § 3.4, and § 3.5 for details). Table 4 gives the adopted extinctions to the galaxies and the methods used to determine them (§ 3.2) in columns (2) and (3). Column (4) lists the dereddened Brγ luminosities (§ 3.4), and column (5) the Brγ equivalent widths (§ 3.7). Columns (6) and (7) list the dereddened 1–0 $S(1)$ luminosities and equivalent widths (§ 3.7).

3.2. *Extinction Corrections*

To derive line luminosities, we must determine correction factors for extinction within the galaxies. The preferred method was to use $E(B-V)$ values from Veilleux et al. (1994). For galaxies they did not observe or for which they were unable to calculate this quantity, we tried to obtain measurements of the $J-H$ and $H-K$ colors from the literature and then dereddened the colors to those of normal elliptical galaxies ($J-H = 0.68$ and $H-K = 0.20$; see Frogel et al. 1978). For Mrk 231, whose red colors suggest significant nonstellar emission, we used only the $J-H$ color for dereddening, since longer wavelengths are more severely contaminated by hot dust emission than shorter wavelengths. The extinction to IRAS 09111−1007 was derived from a measurement of the Paα/Brγ ratio, assuming an intrinsic case B ratio of 12.35 at temperature of 5000 K and density of 10^3 cm^{-3} (Hummer & Storey 1987). For IRAS 09111−1007, the measured Paα flux was $(33.5 \pm 0.7) \times 10^{-18}$ W m^{-2} μm; the dispersion of the Gaussian fitted to that line was $(2.93 \pm 0.04) \times 10^{-3}$ μm. For the remainder of the galaxies (one ULIBG and four comparison objects) no dereddening was performed.

3.3. *Line Widths*

Using points unaffected by known spectral features, the continuum for each galaxy was fitted with a power law and then subtracted. A second continuum subtraction, to remove residual continuum was peformed for the region containing the 1–0 $S(1)$ and Brγ lines; we avoided the potential H_2 2–1 $S(2)$ emission line and Mg, Al, Si, and Ti absorption features (see Fig. 2 for positions). Finally, a χ^2 minimization routine (Bevington 1969) was used to fit the four to six points containing the emission lines with a Gaussian line profile, solving for the line center, dispersion, and peak flux density. We caution the reader that the uncertainties in the line widths, given in Table 3, are not always Gaussian. This is due to the way the uncertainties were calculated; the software fixed all parameters except for the line width, which was varied until the χ^2 of the fit increased by 1.0. However, if the fit's χ^2 is appreciably greater than 1.0 to begin with, the errors in the fitted parameters become non-Gaussian.

No ULIBG had a 1–0 $S(1)$ line broader by 2 σ than the instrumental profile. In only two ULIBGs, IRAS 05189−2524 and Mrk 231, did we observe Brγ lines broadened more than 2 σ beyond the instrumental profile ($\sigma_{arc} = 3.18 \times 10^{-3}$ μm $\approx$ 450 km s^{-1} at 2.2 μm; this is the dispersion expected for

TABLE 3

OBSERVED EMISSION-LINE FLUXES AND LINE WIDTHS

Galaxy (1)	Brγ (10^{-18} W m^{-2}) (2)	σ (10^{-3} μm) (3)	1-0S(1) (10^{-18} W m^{-2}) (4)	σ (10^{-3} μm) (5)
ULTRALUMINOUS GALAXIES				
IRAS 05189 −2524	13.1 ± 1.5	4.02 ± 0.29	6.1 ± 1.0	2.84 ± 0.32
IRAS 08572 +3915	0.7 ± 0.2	1.74 ± 0.32	1.4 ± 0.3	3.04 ± 0.47
IRAS 09111 −1007	3.0 ± 0.5	2.76 ± 0.28	4.0 ± 0.5	2.51 ± 0.23
IRAS 10565 +2448	10.0 ± 0.3	2.66 ± 0.06	7.3 ± 0.3	2.53 ± 0.08
IRAS 12112 +0305	2.8 ± 0.4	3.13 ± 0.36	3.5 ± 0.4	2.71 ± 0.19
Mrk 231	24.7 ± 5.0	6.11 ± 0.94	10.3 ± 3.0	2.59 ± 0.54
Mrk 273	7.3 ± 0.4	2.80 ± 0.11	19.1 ± 0.6	2.95 ± 0.06
IRAS 14378 −3651	2.3 ± 0.4	2.49 ± 0.33	3.0 ± 0.4	3.72 ± 0.35
IRAS 15250 +3609	1.5 ± 0.2	2.55 ± 0.20	1.7 ± 0.2	2.24 ± 0.16
Arp 220	5.9 ± 1.3	2.98 ± 0.47	21.1 ± 1.5	2.50 ± 0.15
IRAS 17208 −0014	5.8 ± 0.4	3.25 ± 0.17	10.7 ± 0.4	2.92 ± 0.07
IRAS 19297 −0406	2.2 ± 0.4	3.31 ± 0.47	2.8 ± 0.5	2.97 ± 0.48
IRAS 23365 +3604	3.4 ± 0.4	3.32 ± 0.30	5.0 ± 0.3	2.61 ± 0.12
COMPARISON SAMPLE GALAXIES				
NGC 695	5.0 ± 0.7	2.71 ± 0.28	3.9 ± 0.7	2.43 ± 0.34
MCG+05-06-036	2.5 ± 0.6	2.03 ± 0.38	7.9 ± 1.1	2.45 ± 0.24
NGC 1068	132.8 ± 34.2	4.13 ± 0.67	126.4 ± 25.4	2.60 ± 0.35
NGC 1614	51.9 ± 4.6	2.87 ± 0.18	10.9 ± 3.3	2.50 ± 0.55
UGC 3094	4.2 ± 0.6	3.53 ± 0.41	3.8 ± 0.6	2.72 ± 0.31
UGC 3608	8.6 ± 0.3	3.75 ± 0.10	5.6 ± 0.3	2.81 ± 0.10
NGC 2342	3.8 ± 0.4	2.99 ± 0.23	2.6 ± 0.4	2.62 ± 0.33
NGC 2388	26.8 ± 2.3	2.87 ± 0.18	19.3 ± 1.8	2.93 ± 0.19
NGC 2623	9.6 ± 0.5	2.71 ± 0.11	12.1 ± 0.6	2.75 ± 0.11
MCG +08-18-012	3.7 ± 0.5	2.12 ± 0.23	3.9 ± 0.4	2.24 ± 0.17
NGC 3110	6.0 ± 0.9	3.74 ± 0.39	3.8 ± 0.7	3.05 ± 0.38
A1101+41	6.1 ± 1.0	2.95 ± 0.29	5.2 ± 0.9	2.96 ± 0.30
MCG +00-29-023	6.1 ± 1.0	3.37 ± 0.42	5.2 ± 0.9	2.75 ± 0.33
Arp 193	13.5 ± 0.5	2.69 ± 0.07	12.1 ± 0.5	2.63 ± 0.07
NGC 5256	8.3 ± 0.5	2.57 ± 0.10	4.3 ± 0.6	2.66 ± 0.29
Zw 247.020	5.2 ± 0.6	2.55 ± 0.24	5.6 ± 0.6	2.23 ± 0.14
I Zw 107	11.2 ± 0.5	2.76 ± 0.09	6.7 ± 0.6	3.35 ± 0.23
NGC 6090	16.0 ± 1.9	2.89 ± 0.24	2.5 ± 1.3	2.03 ± 0.60
IRAS 16164 −0746	6.6 ± 0.9	2.91 ± 0.27	9.5 ± 0.9	3.00 ± 0.18
MCG +01-42-088	8.5 ± 1.6	3.55 ± 0.50	6.5 ± 1.3	4.41 ± 0.75
NGC 6240	18.9 ± 4.5	4.23 ± 0.66	177.4 ± 5.1	4.08 ± 0.08
IRAS 17138 −1017	22.5 ± 0.7	2.86 ± 0.07	12.9 ± 1.2	3.56 ± 0.23
NGC 7469	45.7 ± 2.4	4.05 ± 0.16	18.0 ± 2.3	2.59 ± 0.24
Zw 475.056	3.5 ± 0.7	3.14 ± 0.44	4.2 ± 0.6	2.52 ± 0.28

an unresolved line; the FWHM would be $\sim$1000 km s^{-1}). These galaxies are classified as Seyfert 2 and Seyfert 1 AGNs, respectively, based on their optical spectra (Veilleux et al. 1994). We note that there is no evidence for broad Brγ emission in Arp 220, where DePoy, Becklin, & Geballe (1987) report having observed Brα emission with full width at half maximum (FWHM) velocity of 1300 km s^{-1}. A line this broad convolved with our instrumental function would have a dispersion $\sigma_{\rm line} = 5.15 \times 10^{-3}$ μm, and we can exclude this at the 4.6 σ level. Although the resolution of our spectra allows us to place only upper limits on the intrinsic widths of the Brγ lines, it seems likely that none of the galaxies with an unresolved Brγ line have an intrinsic line width greater than $\sim$1000 km s^{-1} FWHM. Our infrared spectroscopy has revealed no previously unrecognized Seyfert 1 ULIBGs.

3.4. Brγ *Line Strengths*

In Figure 3*a*, we present dereddened Brγ fluxes for the ULIBGs and for the less luminous *IRAS* galaxies. We deredened the Brγ fluxes as described in § 3.2.

To test for a linear relationship between Brγ and infrared luminosity, we performed a linear regression on the data for the comparison objects using routines from Press et al. (1992). Solving for a simple linear function, $\log (L_{\rm Br\gamma}) = a + b \times \log (L_{\rm IR})$ gives $a = -8.66 \pm 2.94$ and $b = 1.33 \pm 0.26$, with $\chi^2 = 1.88$ and Pearson's correlation coefficent $r = 0.74$. In a more physical sense, if a relationship exists where the Brγ luminosity is directly correlated with the infrared luminosity, $L_{\rm Br\gamma} \propto L_{\rm IR}$, then $\log (L_{\rm Br\gamma}) = c + \log (L_{\rm IR})$ [alternatively, $\log (L_{\rm Br\gamma}/L_{\rm IR}) = c$]. We found the mean of the quantity log

TABLE 4

EXTINCTION-CORRECTED LINE LUMINOSITIES

Galaxy (1)	A_K (mag) (2)	Method[a] (3)	$\log(L_{Br\gamma}/L_\odot)$ (4)	EQW(Brγ) (Å) (5)	$\log(L_{S(1)}/L_\odot)$ (6)	EQW(S(1)) (Å) (7)
ULTRALUMINOUS GALAXIES						
IRAS 05189 −2524	0.66	1	7.31	4.0	6.98	1.9
IRAS 08572 +3915	0.38	1	6.23	3.5	6.54	6.8
IRAS 09111 −1007	0.38	3	6.80	5.4	6.92	6.8
IRAS 10565 +2448	0.57	1	7.18	14.	7.04	9.9
IRAS 12112 +0305	0.10	2	6.91	19.	7.01	23.
Mrk 231	0.50	2	7.62	2.8	7.24	1.2
Mrk 273	0.35	1	6.89	8.6	7.30	22.
IRAS 14378 −3651	...	4	6.72	15.	6.83	19.
IRAS 15250 +3609	0.25	1	6.45	7.7	6.50	8.1
Arp 220	1.00	1	6.45	5.0	7.00	18.
IRAS 17208 −0014	0.61	1	6.98	7.6	7.25	14.
IRAS 19297 −0406	0.51	1	7.11	20.	7.22	24.
IRAS 23365 +3604	0.29	1	6.96	12.	7.13	18.
COMPARISON SAMPLE GALAXIES						
NGC 695	0.33	1	6.55	7.8	6.44	5.9
MCG+05-06-036	...	4	6.14	2.1	6.64	6.1
NGC 1068	0.22	1	6.10	3.2	5.97	2.6
NGC 1614	0.32	1	6.91	21.	6.23	4.0
UGC 3094	...	4	6.10	4.5	6.06	4.0
UGC 3608	...	4	6.32	21.	6.13	13.
NGC 2342	...	4	5.77	6.4	5.61	4.2
NGC 2388	0.44	1	6.59	7.7	6.45	5.4
NGC 2623	0.46	2	6.42	8.1	6.52	11.
MCG +08-18-012	0.37	1	6.27	5.9	6.30	5.9
NGC 3110	0.29	1	6.02	6.8	5.83	4.1
A1101+41	0.30	2	6.70	9.1	6.63	7.4
MCG +00-29-023	0.47	1	6.46	6.0	6.39	5.0
Arp 193	0.45	1	6.78	21.	6.73	18.
NGC 5256	0.16	1	6.60	12.	6.32	6.0
Zw 247.020	0.47	1	6.48	6.8	6.51	6.9
I Zw 107	0.57	1	7.21	29.	6.99	17.
NGC 6090	0.19	1	6.94	30.	6.14	4.6
IRAS 16164 −0746	0.54	1	6.45	12.	6.61	17.
MCG +01-42-088	0.48	1	6.60	11.7	6.48	8.7
NGC 6240	0.53	1	6.99	7.7	7.96	71.
IRAS 17138 −1017	0.32	2	6.70	17.	6.46	9.3
NGC 7469	0.00	1	6.79	7.4	6.39	2.9
Zw 475.056	0.37	1	6.28	4.5	6.35	5.3

[a] Methods for extinction determination were as follows: (1) $E(B-V)$ from Veilleux et al. 1994; (2) $H-K$ ($J-H$ for Mrk 231); (3) Paα/Brγ, this paper; (4) no estimate of extinction possible owing to lack of colors and line ratios.

($L_{Br\gamma}/L_{IR}$) to be -4.93 ± 0.24. In terms of L_{FIR}, we find $\log(L_{Br\gamma}/L_{FIR}) = -4.81 \pm 0.26$.

This finding is consistent with a similar relationship found by DePoy (1987) between Brα and L_{FIR} for a sample of lower luminosity *IRAS* galaxies and H II regions, especially given differences in aperture between the two sets of measurements; using case B recombination theory (with $T = 5000$ K and $n_e = 10^4$ cm^{-3} and recombination intensities from Hummer & Storey 1987), his relationship becomes $\log(L_{Br\gamma}/L_{FIR}) = -4.46$. Veilleux et al. (1994) found values of $\log(L_{H\alpha}/L_{IR})$ of ~ -2.5 to -3.5, entirely consistent with a case B extrapolation of our $L_{Br\gamma}/L_{IR}$ ratio, which results in a predicted $\log(L_{H\alpha}/L_{IR})$ of -2.96 (as above, using values from Hummer & Storey 1987).

These relationships do not hold for the non-Seyfert ULIBGs, as may be seen in Figure 3*a*. For their infrared luminosities, the ULIBGs not known to contain AGNs are deficient in Brγ photons relative to less luminous *IRAS* galaxies. We now consider 10 of the 13 ULIBGs, excluding IRAS 05189−2524 and Mrk 231, which are "warm" sample AGNs, and IRAS 14378−3651, for which no extinction estimate is available. Of these 10 systems, five galaxies have $L_{Br\gamma}/L_{IR}$ ratios equal to or lower than any comparison object for which the extinction was determined (the galaxies are IRAS 08572+3915, IRAS 12112+0305, IRAS 15250+3609, Arp 220, and IRAS 17208−0014). A Mann-Whitney *U*-test shows that these 10 ULIBGs, as a group, have lower $L_{Br\gamma}/L_{IR}$ ratios than the less luminous galaxies at the 3.18 σ (probability >0.998) level of confidence.

We do not believe that aperture effects are responsible for the Brγ deficiency of the ULIBGs. Our aperture has the smallest physical dimensions (in square kiloparsecs) for the closer, less luminous galaxies and the largest for the distant, higher

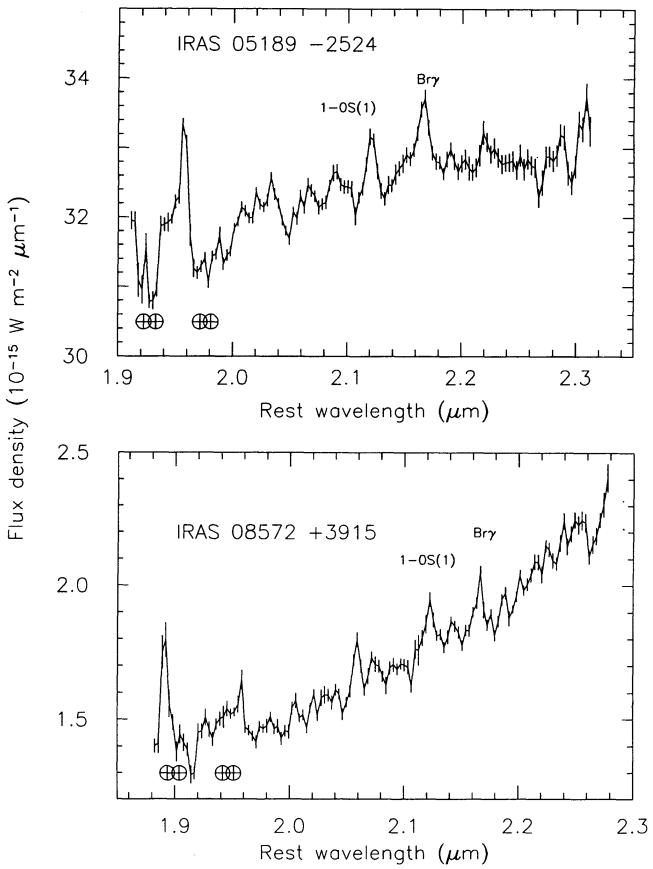

FIG. 1*a*

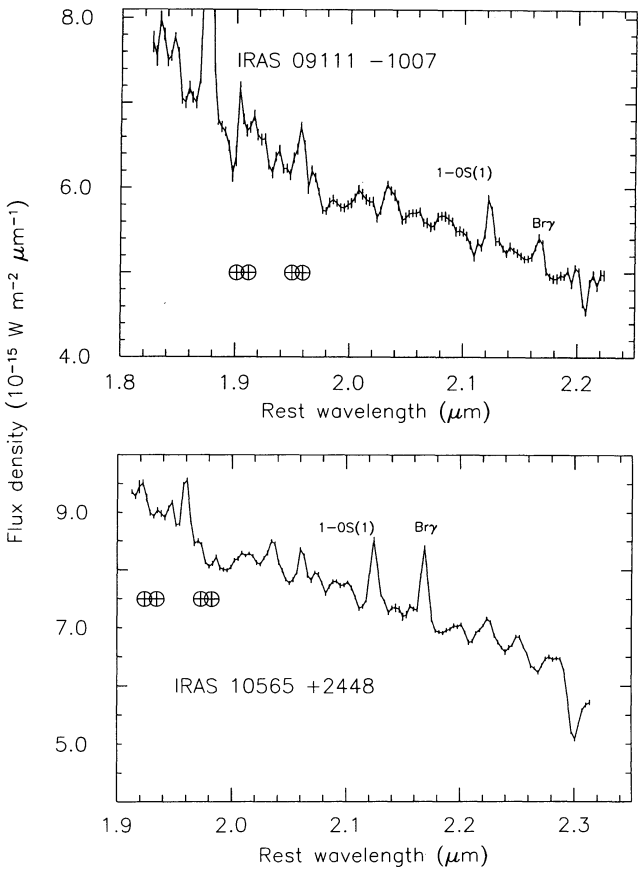

FIG. 1*b*

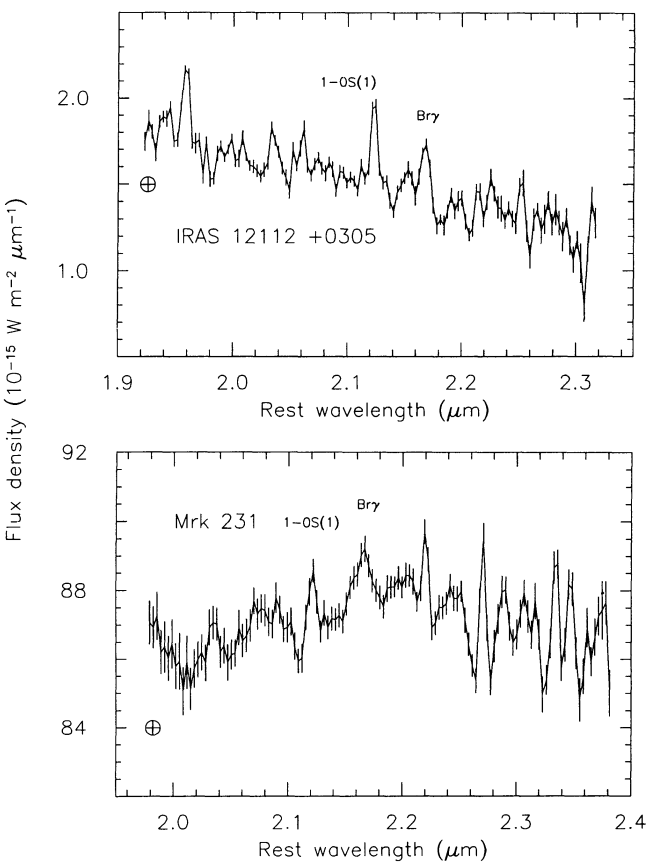

FIG. 1*c*

FIG. 1.—Observed spectra of ultraluminous *IRAS* galaxies. The spectra have been shifted to rest frame using the velocities given in Table 1. The positions of strong Telluric CO absorption lines have been identified. The H_2 $v = 1$–0 $S(1)$ line is at 2.122 μm, and Brγ is at 2.166 μm. The strong line at the blue end of the spectrum of IRAS 09111 − 1007 is Paα.

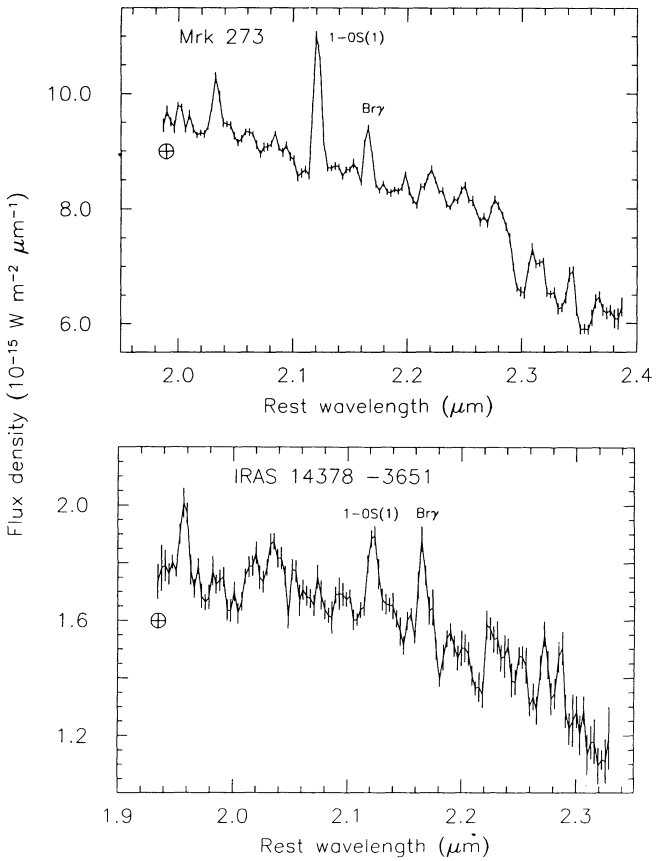

FIG. 1*d*

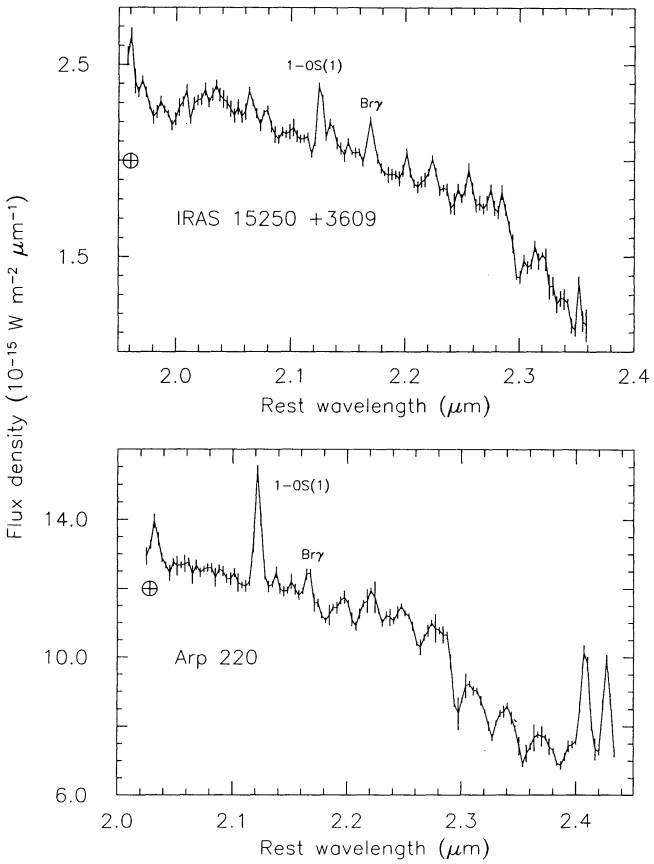

FIG. 1*e*

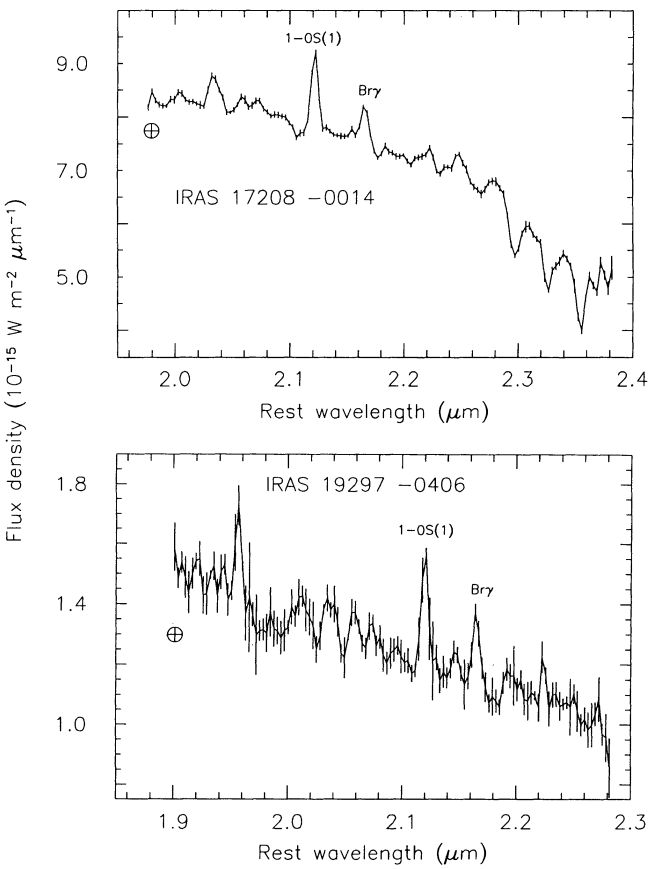

FIG. 1*f*

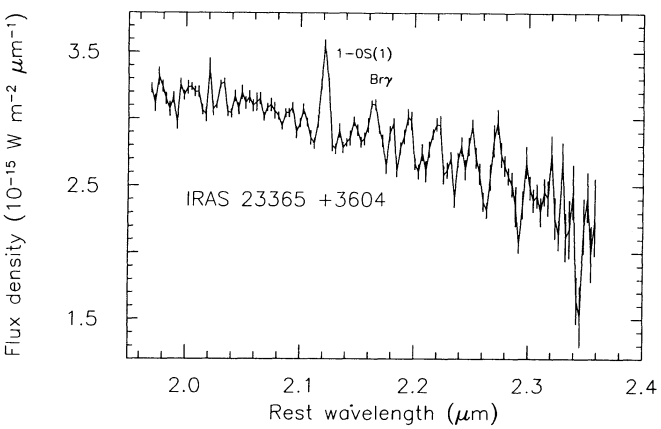

FIG. 1*g*

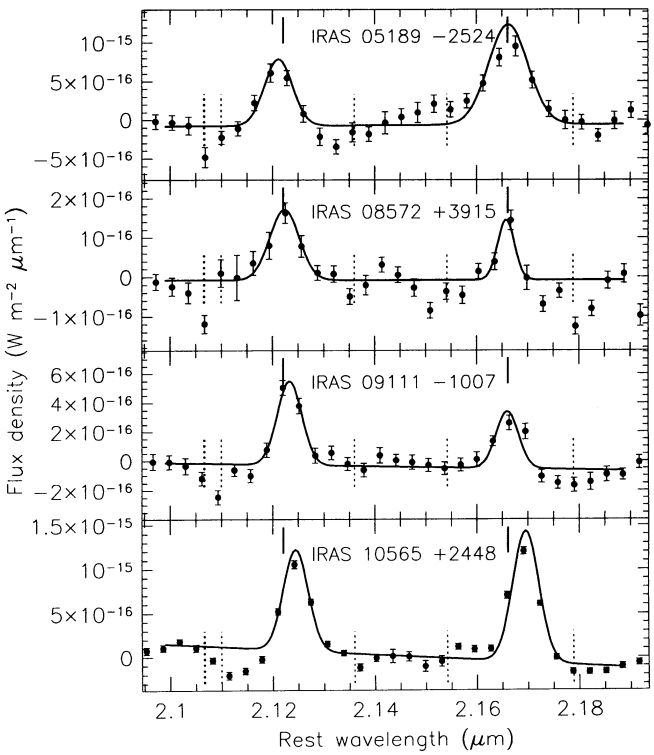

FIG. 2*a*

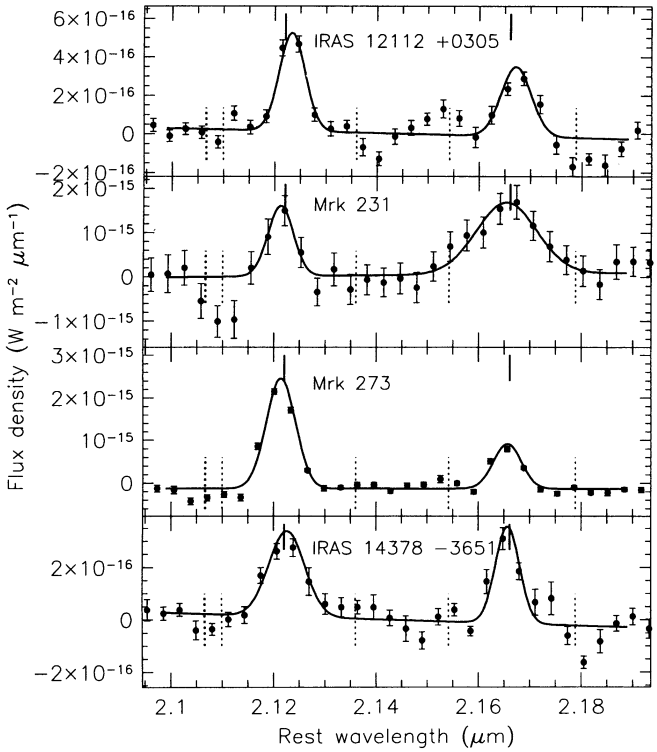

FIG. 2*b*

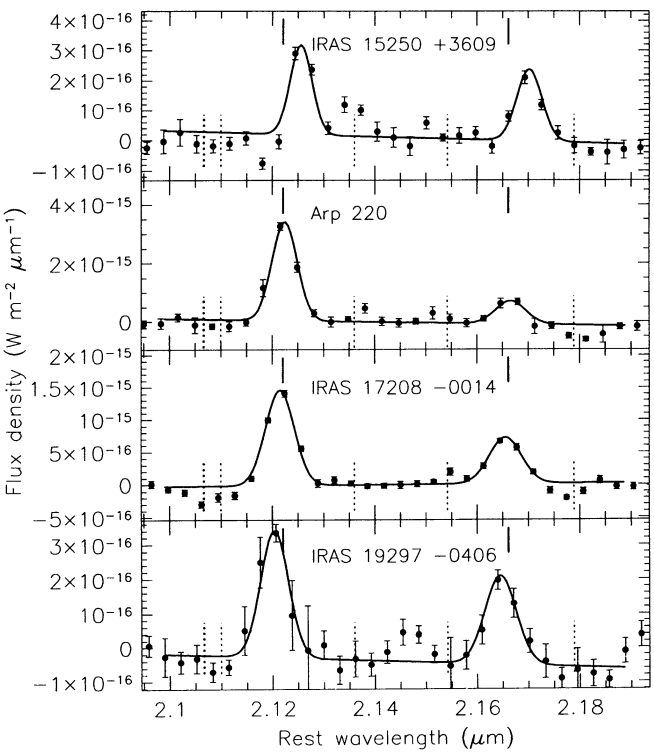

FIG. 2*c*

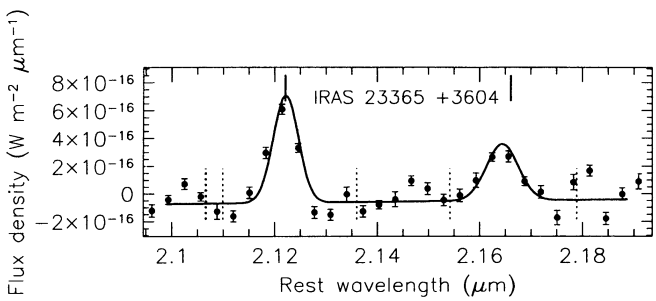

FIG. 2*d*

FIG. 2.—Fits to the 1–0 $S(1)$ and Brγ lines in the ultraluminous galaxies. The continuum has been subtracted to first order for the spectra presented here. The dark lines are the sum of the residual continuum and line fits. The dark vertical lines mark the positions of 1–0 $S(1)$ and Brγ; the dotted vertical lines mark the positions of the stellar metal lines which were avoided for purposes of obtaining the line fits.

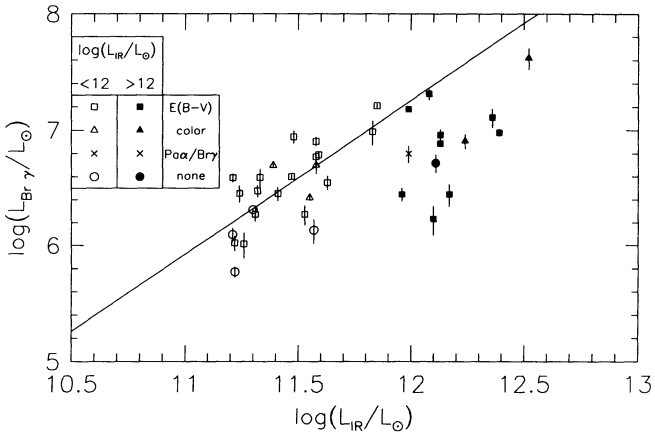

FIG. 3a

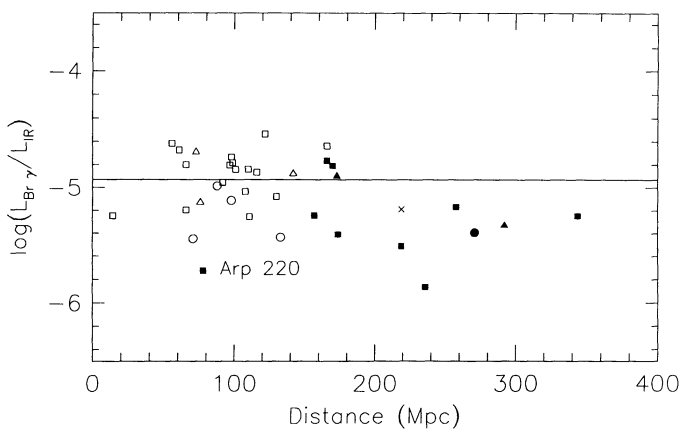

FIG. 3b

FIG. 3.—(*a*) Dereddened Brγ line strength is plotted against infrared luminosity. The open points are the lower luminosity galaxies, the filled points are the ultraluminous galaxies, and the different point styles show the dereddening method used for each galaxy. The fit to the lower luminosity galaxies, $\log (L_{\mathrm{Br}\gamma}) = -8.66 + 1.33 \times \log (L_{\mathrm{IR}})$, is shown. Notice how the ultraluminous galaxies fall systematically below the fit compared to the lower luminosity galaxies. (*b*) The Brγ/infrared ratio is shown as a function of distance. The solid line assumes a linear relationship between $L_{\mathrm{Br}\gamma}$ and L_{IR}: $\log (L_{\mathrm{Br}\gamma}/L_{\mathrm{IR}}) = -4.93$. If aperture effects were important, we would expect a line with positive slope to fit better than the zero-slope line plotted.

luminosity systems (3″ = 1.5 kpc at 100 Mpc). If aperture effects were significant, we would expect the nearby galaxies, not the distant ones, to show low $L_{\mathrm{Br}\gamma}/L_{\mathrm{IR}}$ ratios. This is opposite the trend observed in the data (Fig. 3*b*).

In summary, *for their infrared liminosities, the 10 ULIBGs in this sample not previously classified as AGNs are, as a group, deficient in Brγ photons relative to less luminous infrared galaxies.*

3.5. *Molecular Hydrogen Line Strengths*

In Figure 4*a*, dereddened 1–0 $S(1)$ luminosities for the ULIBGs are plotted against their far-infrared luminosities. The line measurements were dereddened using the methods outlined in § 3.2; the method used for each galaxy is noted in Table 4.

As we did with the Brγ line strengths, we performed a linear regression analysis on the $S(1)$ data for the comparison objects. Solving for $\log (L_{S(1)}) = a + b \times \log (L_{\mathrm{IR}})$ gives $a = -7.12 \pm 3.25$ and $b = 1.18 \pm 0.28$, with $\chi^2 = 1.12$ and Pearson's correlation coefficient $r = 0.67$. These findings are consistent with an intrinsic, more physical relationship where the $S(1)$ luminosity is directly correlated with the infrared luminosity, $L_{S(1)} \propto L_{\mathrm{IR}}$, or $\log (L_{S(1)}/L_{\mathrm{IR}}) = c$. As before, we then found the mean value and standard deviation of the constant c to be $c = -5.07 \pm 0.23$. In terms of L_{FIR}, we find $\log (L_{S(1)}/L_{\mathrm{FIR}}) = -4.95 \pm 0.22$. The thirteen ULIBGs follow a similar relation; they lie along the line established by the lower luminosity galaxies in Figure 5*a*. Including both the ULIBGs and comparison sample galaxies in the fit yields a relation $\log (L_{S(1)}/L_{\mathrm{IR}}) = -5.11 \pm 0.22$. This is essentially identical to the findings of Joseph et al. (1987), who found $\log (L_{S(1)}/L_{\mathrm{FIR}}) = -5$. Again, this is not an aperture effect, as Figure 4*b* shows.

3.6. Brγ *and* 1–0 $S(1)$ *Equivalent Widths*

Equivalent widths enable us to examine the relative strengths of emission features to the nearby continuum. We

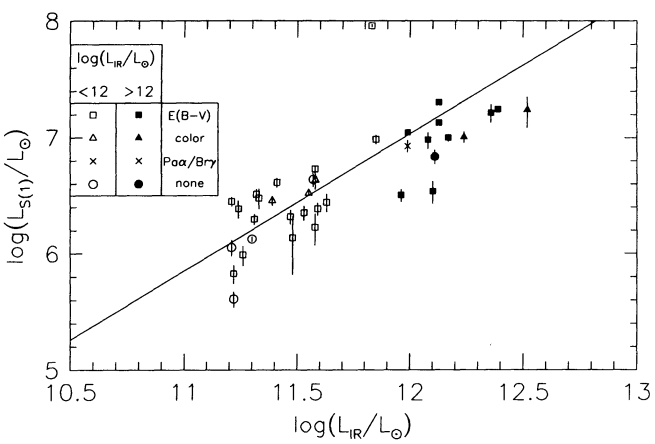

FIG. 4a

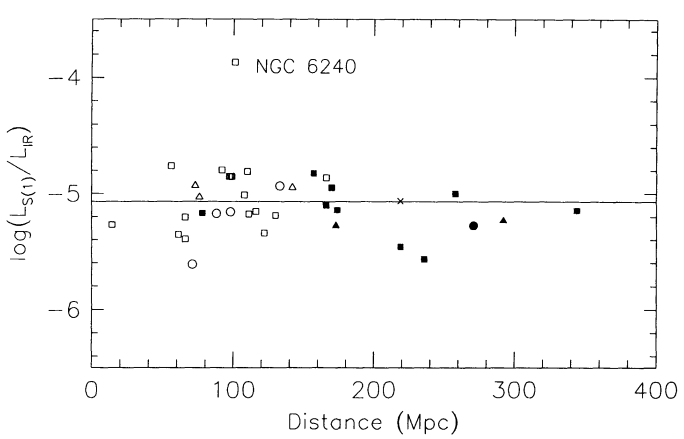

FIG. 4b

FIG. 4.—(*a*) Dereddened 1–0 $S(1)$ line strength is plotted against infrared luminosity. The open points are the lower luminosity galaxies, the filled points are the ultraluminous galaxies, and the different point styles show the dereddening method used for each galaxy. The fit to the lower luminosity galaxies is shown, $\log (L_{S(1)}) = -7.12 + 1.18 \times \log (L_{\mathrm{IR}})$. (*b*) The $S(1)$/infrared ratio is shown as a function of distance. The solid line assumes a linear relationship between $L_{S(1)}$ and L_{IR}, or $\log (L_{S(1)}/L_{\mathrm{IR}}) = -5.07$. If aperture effects were important, we would expect a line with positive slope to fit better than the zero-slope line plotted.

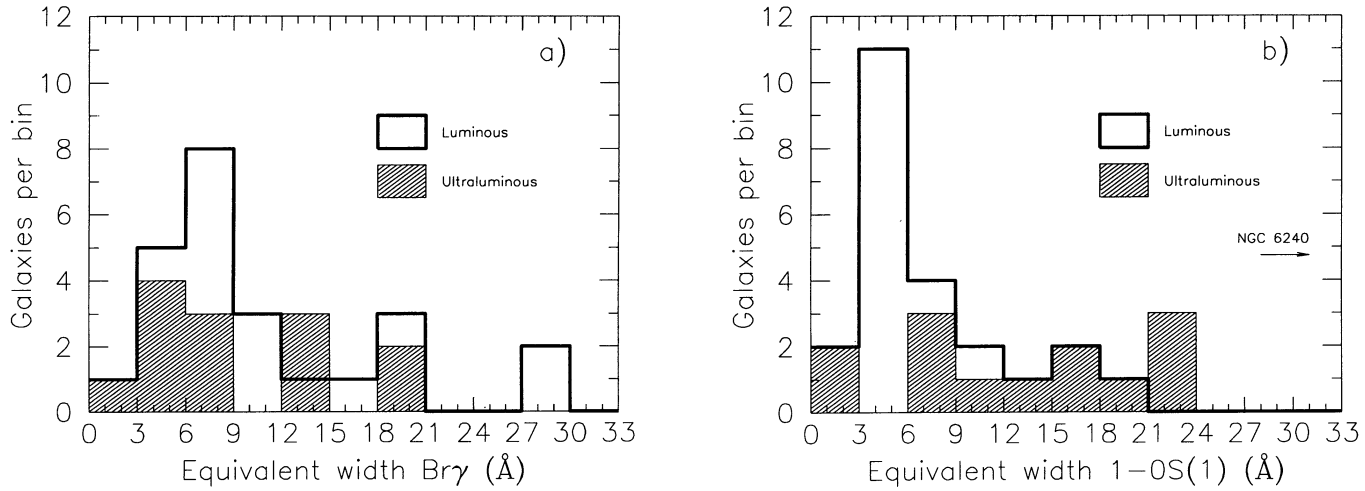

FIG. 5.—(*a*) Histogram of Brγ equivalent widths. (*b*) Histogram of H_2 1–0 *S*(1) equivalent widths

have defined the equivalent widths of the emission lines as the ratio of the integrated line fluxes to the local continuum flux densities.

In Figure 5*a*, we have plotted a histogram of the equivalent widths of the Brγ lines for the ULIBGs and the comparison objects. Brγ equivalent widths range from ~3–30 Å. The samples appear to follow similar or identical distributions. We note that the six galaxies in Table 1 that Veilleux et al. (1994) classified as AGNs are in the lowest three bins (one each in the first and third bins, four in the second).

Figure 5*b* shows the histogram of 1–0 *S*(1) equivalent widths. It strongly suggests that the ULIBGs and the lower luminosity galaxies follow different distributions. The lower luminosity galaxies follow a narrow distribution peaked around 3–9 Å, whereas the ULIBGs follow a very broad distribution extending to much larger equivalent widths. NGC 6240 remains not only the most luminous galaxy in *S*(1) emission, but it also has the highest equivalent width, 71 Å. The ULIBG AGNs IRAS 05189−2524 and Mrk 231 are again located in the lowest bin; two of the three lower luminosity AGNs are in the lowest bin, the third (Zw 475.056) is in the second bin. Again, the AGNs have among the lowest equivalent widths in the two samples. Marconi et al. (1994) found a similar result for the AGNs in their sample. But while they suggested that the low equivalent widths were due to a lack of emitting H_2 gas, our results indicate that the H_2 lines are as strong as we would expect in the AGNs–in other words, these galaxies follow the same relation between $L_{S(1)}$ and L_{IR} as the other galaxies, and so the lines are *not* weak. The low equivalent widths, our data suggest, are due to the AGNs having more luminous continua, not weaker line emission, than the starbursts.

3.7. *Absolute Magnitudes*

We have used our spectra to compute spectrophotometric *K* magnitudes from the 2.2 μm rest frame flux densities of the galaxies and transformed these into absolute magnitudes, M_K. The absolute magnitudes before correction for extinction are shown in Figure 6*a*, while Figure 6*b* shows the effects of correction for the extinction listed in Table 4; the magnitudes themselves, following the extinction corrections, are listed in Table 2. Figure 6*b* shows what appears to be a cutoff in absolute magnitude; excluding the two ULIBG AGNs (Mrk 231, with $M_K = -27.53$, and IRAS 05189−2524, with $M_K = -26.53$), no ULIBG or lower luminosity galaxy is brighter than $M_K = -25$. Except for the two ULIBG AGNs, almost all the ULIBGs seem to have an absolute magnitude of ~ -23.5, with a scatter (likely partially due to aperture effects) of ~1 mag. A trend between M_K and L_{IR} may exist for the lower luminosity galaxies, which follow a linear relation between *K*-band and infrared luminosities: $M_K = -2.5 \log (L_{IR}/L_\odot) + c$, where $c = 5.03 \pm 0.52$. The ULIBGs as a group do not appear to follow this trend.

It seems that *K*-band luminosity does not scale linearly with L_{IR}. This is probably the same effect found by Soifer et al. (1987) for blue luminosity among the original BGS objects. That the ULIBGs fall somewhat below the relation defined by the lower luminosity galaxies may indicate that the extinctions given in Table 4 are still underestimated.

Of the 10 ULIBGs without broad lines (IRAS 05189−2524 and Mrk 231) or extinction measurements (IRAS 14378−3651), eight have smaller L_K/L_{IR} ratios than any of the comparison sample objects with measured extinctions.

3.8. CO *Indices*

The CO indices of the galaxies were computed using the method given in § 2 and are shown graphically in Figure 7. Five of the ULIBGs were at distances so large that the CO band heads were redshifted out of the *K* band. However, the histograms of the photometric CO indices in Figure 7 show that the ULBIGs and comparison objects follow approximately the same distributions. The two ULIBG AGNs IRAS 05189−2524 and Mrk 231 have the lowest CO indices of any galaxies we measured; the comparison sample AGN NGC 7469 also is notable for a low CO index, much as seen with the emission-line equivalent widths earlier in this section.

Frogel et al. (1978) found $CO_{ph} = 0.13$–0.18 in a sample of elliptical galaxies. That we found many galaxies with higher values indicates that the stars responsible for the 2 μm continua of these galaxies are either of later spectral type or of a more luminous class than the average spectral types of the ellipticals observed by Frogel et al. (1978). The 2 μm continua of the galaxies with the deep CO indices are dominated by light from stars later or more luminous than K giants, such as M giants or K or M supergiants. A 2 μm continuum dominated by late-type giants implies a stellar population at least ~10 Gyr old, which is inconsistent with the evidence of ongoing star forma-

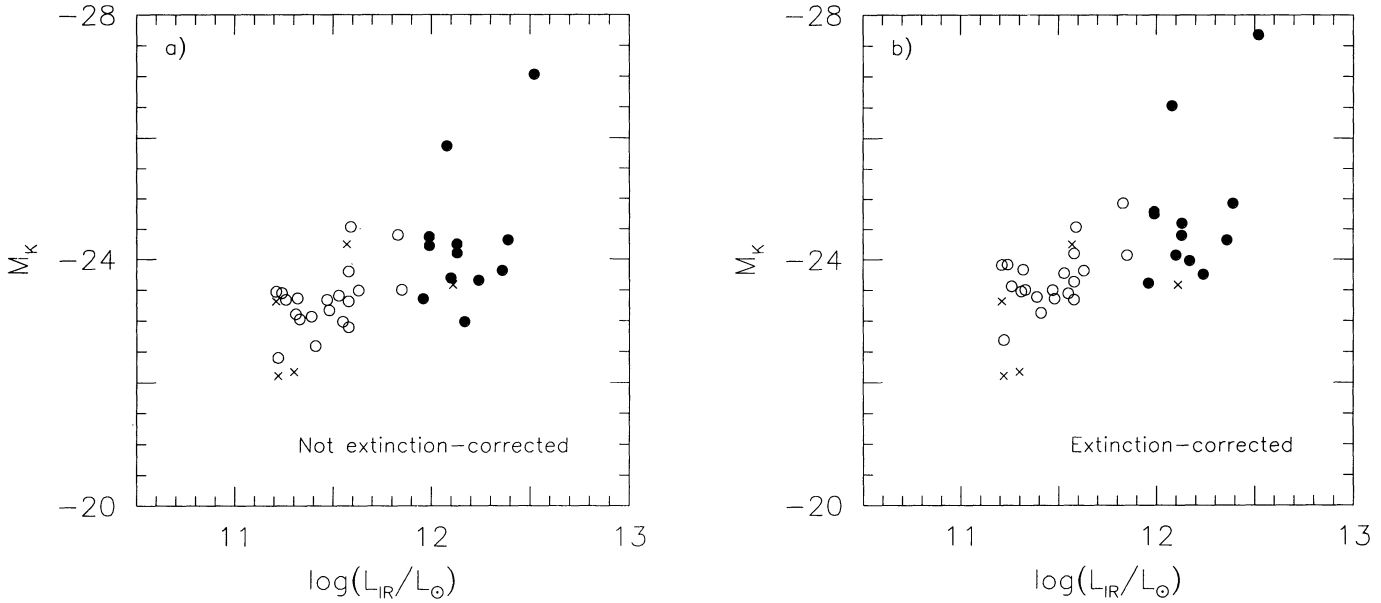

FIG. 6.—(*a*) Absolute *K*-band magnitudes for the ultraluminous and lower luminosity galaxies (*filled* and *open circles*, respectively; *crosses* denote galaxies for which no extinction estimates are available), plotted against the infrared luminosity. The magnitudes have *not* beeen corrected for extinction. (*b*) As in (*a*), *after* correction for extinction.

tion. On the other hand, a 2 μm continuum arising from K and M supergiants is entirely consistent with the presence of a starburst several tens of millions of years old. This is firm evidence that the stellar populations of luminous infrared galaxies are significantly different than those of normal galaxies not selected on the basis of their infrared luminosities.

The red power-law indices of the broad-line AGNs, much redder than normal starlight, as well as the galaxies' very bright values of M_K, show that their continua are not dominated by reddened starlight. These objects have 2 μm continua that contain a significant fraction ($\geq 50\%$) of nonstellar emission, from either hot dust at temperatures of ~ 500–2000 K or power-law nonthermal emission from the AGNs themselves. It is therefore expected that such AGNs (and especially Seyfert 1 galaxies) will have unusually small CO indices.

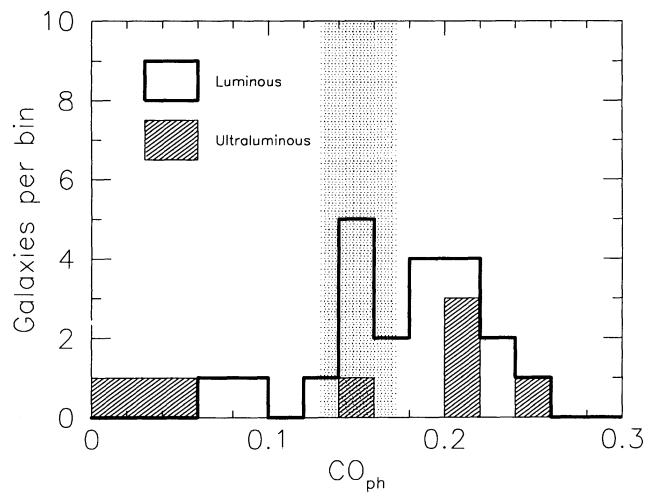

FIG. 7.—Histogram of photometric CO indices. The range of normal ellipticals, which have values of CO_{ph} near 0.15 (Frogel et al. 1978), is indicated by the vertical gray stippled region.

3.9. *Summary of Spectral Features*

We can summarize the properties of the ULIBGs and the lower luminosity objects in a comparative fashion.

Ten of the ULIBGs generally have Brγ equivalent widths similar to the comparison sample but a greater potential to exhibit large *S*(1) equivalent widths. They have, on average, CO indices similar to or slightly stronger than the comparison sample galaxies. Their $L_{Br\gamma}/L_{IR}$ ratios are less than for the lower luminosity galaxies, but the $L_{S(1)}/L_{IR}$ ratios are similar. These ULIBGs tend to have moderate power laws ($\beta \sim -2.4$ to -1.4), not so steep as for the comparison sample objects.

Two of the ULIBGs (IRAS 05189−2524 and Mrk 231) appear to be AGNs. They have small equivalent widths for both Brγ and 1–0 *S*(1), as well as weaker CO absorption than the other galaxies. These galaxies have red power laws and very strong emission at 2 μm, which results in these galaxies having redder, more luminous near-infrared continua than the other galaxies. It appears that a substantial portion of the 2 μm continuum of these galaxies is nonstellar in origin. Despite this, they follow the same $L_{Br\gamma}/L_{IR}$ and $L_{S(1)}/L_{IR}$ relations as the comparison sample galaxies (it is noteworthy that the comparison sample AGNs, NGC 1068 and NGC 7469, also follow these relations).

The final ULIBG is IRAS 08572+3915, which has the reddest 2 μm continuum and the faintest $L_{Br\gamma}/L_{IR}$ and M_K/L_{IR} ratios of any galaxy we observed. This object appears to derive most of its *K*-band continuum from hot dust or other nonstellar sources.

The comparison sample galaxies have moderate to high Brγ equivalent widths, roughly equal to those of the ULIBGs. However, the comparison objects show *S*(1) equivalent widths clustered between 3 and 15 Å, with less range than the ULIBGs. The comparison galaxies follow a relation between hydrogen recombination line luminosity and infrared luminosity found by us and others, and also have their *S*(1) line strengths proportional to their infrared luminosities (it is again noteworthy that two broad-line AGNs in the comparison

sample, NGC 1068 and NGC 7469, also follow these relations). They have CO indices similar to those of the ULIBGs, but their power-law indices tend to be somewhat smaller, ranging from -3 to -1.4.

4. DISCUSSION

4.1. *A Self-consistent Model for Ultraluminous Infrared Bright Galaxies*

We now present arguments based on our own data and those of other authors that all point to a self-consistent picture of the physical processes occurring in the ULIBGs, and we examine the implications of the following simple model: we believe that the ULIBGs contain very compact nuclei that are typically optically thick at 2 μm. For these objects, the Brγ and K continua from the central luminosity source(s) are highly obscured, resulting in the poor correlations between Brγ, M_K, and L_{IR} for the ULIBGs that were presented in §§ 3.4 and 3.7. The H_2 1–0 $S(1)$ emission then comes from optically thin molecular gas spatially distinct from the central cores. For these objects, we cannot say what fraction of the central luminosity comes from optically thick starbursts, active nuclei, or both. However, in at least some galaxies (Mrk 231 and IRAS 05189−2524) we have a relatively clear line of sight to nuclei containing luminous AGNs, as characterized by broad emission lines and strong nonstellar emission at 2 μm.

In § 3, it was shown that there exists a correlation between hydrogen recmbination line flux and L_{IR} (this work, DePoy 1987, and Veilleux et al. 1994) which holds up to $L_{IR} \simeq 10^{12}\ L_\odot$ and does not hold at higher luminosities: the ULIBGs with starburst-like spectra have a tendency to be underluminous in Brγ. A similar relationship seems to hold for K-band absolute magnitudes and L_{IR}, but again, the ULIBGs tend to be fainter, for their total infrared luminosities, than the less luminous systems. Also, there appears to be a near-universal correlation between $S(1)$ luminosity and L_{IR}. This suggests that the $S(1)$ emission line arises in regions of low optical depth and that its strength is dependent on the infrared luminosity of the host galaxy.

High-resolution VLA observations led CHYT to propose a model in which the nuclei of the more luminous *IRAS* galaxies contained compact starbursts so dense as to be optically thick at radio wavelengths. Those authors predicted independently what we have in fact observed: hydrogen recombination line fluxes could be a poor indicator of infrared activity for those galaxies with dense starbursts in their centers. The model of CHYT implies that optical and near-infrared continua from the stars in these nuclei should be diminished as well.

Enormous optical depths at visual and near-infrared wavelengths are implied by high–spatial resolution submillimeter measurements of molecular gas concentrations in luminous *IRAS* galaxies. Depending on the geometry of the gas, the extinctions implied by the submillimeter measurements imply that the obscurations might even approach 1000 visual magnitudes (Scoville et al. 1991).

Our hypothesis that the Brγ and $S(1)$ emission arises in spatially distinct regions is well supported by observations in the literature (however, these observations are not of *ultraluminous IRAS* galaxies, for which the proper data are not yet available in the literature). Studies of many different galaxies, among them NGC 6240 (Elston & Maloney 1990), NGC 1808 (Krabbe, Sternberg, & Genzel, hereafter KSG), NGC 1068 (Rotaciuc et al. 1991), and NGC 7552 (Forbes, Kotilainen, & Moorwood 1994) show significant differences in the positions of the peaks of the $S(1)$ and Brγ lines. We expect this trend to continue when observations of the ULIBGs are obtained.

Additional evidence in favor of our model for the ULIBGs comes from comparisons of our data with published starburst models. A simple starburst model can be described by only a few parameters: the form of the initial mass function (IMF, assumed to be a power law of the stellar mass), the age of the starburst and star formation rate, the upper and lower mass cutoff values of the IMF (M_u and M_l), and the total luminosity of the starburst. We use as the reference the model of KSG with a 50×10^6 yr old starburst following an IMF with power-law index -2.5, a constant star formation rate, and $M_l = 1\ M_\odot$. We assume that L_{IR} is approximately equal to the bolometric luminosity of the starbursts—a reasonable assumption for the galaxies in question. The chief variable in our comparison then becomes M_u.

We derived a value of $\log (L_{Br\gamma}/L_{IR}) = -4.93 \pm 0.24$ from our observations of the comparison sample galaxies. KSG predict, for upper mass cutoffs of 50, 40, and 30 $M_\odot$, values of -4.54, -4.68, and -4.91, respectively, and the latter is in good agreement with our empirically determined value. *Our data appear to rule out very high upper mass limits (above 50 $M_\odot$, 2 σ) for the ULIBGs.* Second, KSG predict a relationship between the 2.2 μm and total infrared luminosities for starbursts. In terms of M_K and L_{IR}, we found that $M_K = -2.5 \log (L_{IR}) + (5.03 \pm 0.52)$ for the comparison galaxies. KSG find values of 5.37, 4.95, and 4.77 for upper mass limits of 50, 40, and 30 $M_\odot$, respectively. Although there is a large uncertainty, the models agree roughly with $M_u \sim 40\ M_\odot$. We note a strong disagreement with these results for the ULIBGs. The lower values of $L_{Br\gamma}/L_{IR}$ we found for the ULIBGs favor *low* upper mass cutoffs, 30 $M_\odot$ or less, but the values of M_K/L_{IR} favor *high* upper mass cutoffs, much higher than 50 $M_\odot$. These results are contradictory, and indicate that *low-extinction simple starburst models alone cannot satisfactorily explain the observed properties of the ULIBGs.* If, however, the Brγ and K-band continuum emission from star formation in the ULIBGs arises principally in regions of high optical depth, then these galaxies would obey intrinsically the same correlations as the lower luminosity systems and therefore would be well described by the same starburst models. *Unaccounted-for* extinctions of $\sim$0.8–1.5 mag at K would boost the $L_{Br\gamma/L_{IR}}$ and M_K/L_{IR} ratios of the ULIBGs enough to account for their L_{IR} using starbursts alone. This requires 50%–75% of the Brγ and K-band continuum fluxes to be totally hidden from our view, even after correcting for directly measurable extinction.

4.2. *The Nature of Ultraluminous Infrared Bright Galaxies*

It seems nearly certain that all ULIBGs are mergers of two gas-rich spiral galaxies (e.g., Joseph & Wright 1985; Sanders et al. 1988a; Scoville et al. 1991). Typically, ULIBGs have $>50\%$ of their $\sim 10^{10}\ M_\odot$ of molecular gas located in a diameter of $\sim$1 kpc (Sanders, Scoville, & Soifer 1991; Scoville et al. 1991; Planesas, Mirabel, & Sanders 1991).

The concentration of gas in the central regions results in tremendous column densities averaged over the inner kiloparsec of the galaxy (i.e., in a typical beam for submillimeter measurements). If this gas were homogeneously distributed over the entire beam, the inferred extinctions are on the order of 100 mag A_V, assuming a gas/dust ratio similar to that found for the solar neighborhood (e.g., Scoville et al. 1991; Planesas et al. 1991). For the ULIBG with the best spatial

resolution (in parsecs), Arp 220, the extinction to the center would be $A_V \sim 1000$ mag (Scoville et al. 1991), but since we see both of the radio nuclei at near-infrared wavelengths (Graham et al. 1990), the extinction cannot be so high on all lines of sight, and so the gas cannot be homogeneously distributed. The gas must, rather, be distributed in a highly nonuniform fashion, perhaps in a disk (as Scoville et al. 1991 suggest) or in clumps of density much higher than the beam-averaged density of the molecular gas, with a small volume filling factor in the nucleus. However the gas is actually distributed, any process depending on that gas, whether it is star formation or the fueling of an active nucleus, will stand a high probability of being obscured partially or even totally at optical and near-infrared wavelengths. Further, this absorption would be so total that the light arising in regions at high optical depths would not be reddened or scattered, but rather simply removed from the beam, and the photons themselves would be reprocessed to much longer far-infrared wavelengths owing to multiple absorptions and reemissions. This leads to a natural explanation for two of our principal findings: the deficits of Brγ and K-band continuum emission in the ULIBGs. Since the light we do see would come from the regions at low optical depths, the simple foreground screen geometry generally used for extinction corrections (including those we performed in this paper) is likely to provide an underestimate of the true optical depths to the centers of these galaxies.

4.3. *Implications for the Starburst-AGN Controversy*

Are the ULIBGs powered primarily by starbursts, AGNs, or a mixture of both? It is clear that we still do not see direct evidence for the presence of AGNs in the majority of the ULIBGs. It is also apparent, though, that the extinctions toward the nuclei are so large that, even if AGNs were present in every ULIBG, we should not expect to seem them all. Optical extinctions of $A_V \sim 1000$ mag correspond to $A_K \sim 100$ mag, and even in the mid-infrared, $A_{10\,\mu m} \sim 50$ mag and $A_{20\,\mu m} \sim 20$ mag.

Starbursts and AGNs can obviously coexist in galaxies. For example, the luminous infrared galaxy NGC 7469 has a ring of H II regions around a Seyfert 1 nucleus (e.g., Mazzarella et al. 1994 and references therein), and the circumnuclear region of the ULIBG Mrk 231 (Seyfert 1) seems to be a site of vigorous star formation (e.g., Lípari, Colina, & Macchetto 1994). If the AGNs in such a "composite" galaxy were obscured, such that it appeared as a Seyfert 2, or were even invisible at optical and near-infrared wavelengths, the observed spectrum would be that of the H II regions alone. But, importantly, attenuation of emission from the nucleus (and possibly the H II regions as well) would give the galaxy low $L_{Br\gamma}/L_{IR}$ and a faint M_K/L_{IR}.

Can this be the case for the ULIBGs with relatively weak Brγ and K-band emission? Consider the "prototype" ULIBG, Arp 220, whose $L_{Br\gamma}/L_{IR}$ and M_K/L_{IR} are down by a factor of nearly 7, relative to the lower luminosity galaxies. If this galaxy follows intrinsically the same relations as we found for the lower luminosity LIBGs, we are not detecting fully 85% of the total Brγ and K-band continuum emission. In other words, the near-infrared properties of Arp 220, its Brγ and K continuum strengths, do not seem able to easily explain its high *IRAS* luminosity. It is possible that a powerful AGN, intrinsically much stronger than the observed K-band continuum, is hidden in Arp 220.

The strongest cases for significant obscured AGNs are the galaxies most deficient in $L_{Br\gamma}/L_{IR}$ and M_K/L_{IR}, such as Arp 220, IRAS 08572+3915, and IRAS 15250+3609. In these systems, there could conceivably be a hidden AGN providing the luminosity necessary to make these galaxies obey the correlations found for the comparison sample. It is tantalizing that recent VLBI observations have found evidence that much of the luminosity of Arp 220 may arise in a region of radius ~ 10 pc located in one of its radio nuclei (Lonsdale et al. 1994), that IRAS 15250+3609 is known to contain a VLBI source (Lonsdale, Smith, & Lonsdale 1993), and that IRAS 08572+3915 seems to have a mostly nonstellar 2 μm continuum unique among the ULIBGs. On the other hand, our measurements do allow us to constrain the luminosity of any buried AGN in the other galaxies. Consider systems such as IRAS 10565+2448, which is strong in both Brγ and continuum. Any buried AGN must intrinsically provide emission at 2 μm at most as strong as the observed continuum, or else that galaxy would not intrinsically follow the relations defined by the lower luminosity galaxies.

5. CONCLUSIONS

There are four important results from this initial K-band spectroscopic survey of a sample of 13 ULIBGs.

1. No new broad-line (FWHM > 1000 km s^{-1}) galaxies were discovered among the ULIBGs. If additional such AGN-like objects are indeed present, then the extinctions to the broad-line regions must be at least several tens of visual magnitudes.

2. Three of the 13 galaxies (22%)—the "warm" sample objects IRAS 05189−2524, IRAS 08572+3915, and Mrk 231—show evidence for significant amounts of nonstellar emission at 2 μm; the K-band spectra of the other 10 ULIBGs are dominated by features associated with star formation activity.

3. The CO indices of the ten ULIBGs with starburst-like spectra are stronger than for elliptical galaxies, providing strong evidence that the 2 μm continua of these ULIBGs are dominated by red supergiants in starburst stellar populations.

4. We have direct evidence that most of the ULIBGs are optically thick at 2 μm. If this is true, then our observations do not let us exclude the presence of obscured AGNs capable of providing a large fraction ($\sim$25%–50%) of the total energy output of the 10 ULIBGs with starburst-like K-band spectra. At the same time, the observations themselves do not let us discriminate between compact, optically thick starbursts or buried AGNs as the sources of the "missing" luminosity.

The authors wish to thank the staff of the Joint Astronomy Center and the telescope operators for their excellent service and support and for providing such a wonderful instrument. J. D. G. gratefully acknowledges support from NASA contract NASW-4481. D. B. S. was supported in part by NASA grant NAG5-1741. This research has made use of the NASA/IPAC Extragalactic Database (NED) which is operated by the Jet Propulsion Laboratory, Caltech, under contract with the National Aeronautics and Space Administration.

REFERENCES

Bevington, P. R. 1969, Data Reduction and Error Analysis for the Physical Sciences (New York: McGraw-Hill)
Carico, D. P., Graham, J. R., Wilson, T. D., Soifer, B. T., Neugebauer, G., & Sanders, D. B. 1990, ApJ, 349, L39
Carico, D. P., Sanders, D. B., Soifer, B. T., Elias, J. H., Matthews, K., & Neugebauer, G. 1988, AJ, 95, 356
Catalogued Galaxies and Quasars Observed in the IRAS Survey, 1989, Version 2 (Pasadena: Jet Propulsion Lab.)
Condon, J. J., Helou, G., Sanders, D. B., & Soifer, B. T. 1990, ApJS, 73, 359
Condon, J. J., Huang, Z.-P., Yin, Q. F., & Thuan, T. X. 1991, ApJ, 378, 65 (CHYT)
Condon, J. J., et al. 1994, in preparation
DePoy, D. L. 1987, Ph.D. thesis, Univ. of Hawaii
DePoy, D. L., Becklin, E. E., & Geballe, T. R. 1987, ApJ, 316, L63
De Poy, D. L., Wynn-Williams, C. G., Hill, G. J., & Becklin, E. E. 1988, AJ, 95, 398
Doyon, R., Joseph, R. D., & Wright, G. S. 1994a, ApJ, 421, 101
Doyon, R., Nadeau, D., Joseph, R. D., Goldader, J. D., Sanders, D. B., & Rowlands, N. 1994b, ApJ, submitted
Elston, R., & Maloney, P. 1990, ApJ, 357, 91
Forbes, D. A., Kotilainen, J. K., & Moorwood, A. F. M. 1994, ApJ, 433, L13
Frogel, J. A., Persson, S. E., Aaronson, M., & Matthews, K. 1978, ApJ, 220, 75
Goldader, J. D., Joseph, R. D., Sanders, D. B., & Doyon, R. 1995, in preparation (Paper II)
Graham, J. R., Carico, D. P., Matthews, K., Neugebauer, G., Soifer, B. T., & Wilson, T. D. 1990, ApJ, 354, L5
Hoffleit, D. 1982, The Bright Star Catalogue, (New Haven: Yale Univ. Obs.)
Hummer, D. G., & Storey, P. J. 1987, MNRAS, 224, 801
Johnson, H. L. 1966, ARA&A, 4, 193
Joseph, R. D., & Wright, G. S. 1985, MNRAS, 214, 87
Joseph, R. D., Wright, G. S., & Wade, R. 1984, Nature, 311, 132
Joseph, R. D., Wright, G. S., Wade, R., Graham, J., Gatley, I., & Prestwich, A. 1987, in Star Formation in Galaxies, ed. C. J. Lonsdale Persson (Nasa Conf. Publ. 2466), 421
Kleinmann, S. G., & Hall, D. N. B. 1986, ApJS, 62, 501
Krabbe, A., Sternberg, A., & Genzel, R. 1994, ApJ, 425, 72 (KSG)
Landolt-Börnstein. 1982, Astronomy & Astrophysics, Vol. 2b, Stars and Star Clusters, ed. K.-H. Hellwege, K. Schaifers & H. H. Voigt (New York: Springer)
Lípari, S., Colina, L., & Macchetto, F. 1994, ApJ, 427, 174
Lonsdale, C. J., Diamond, P. J., Smith, H. E., & Lonsdale, C. J. 1994, Nature, 370, 117
Lonsdale, C. J., Smith, H. E., & Lonsdale, C. J. 1993, ApJ, 405, L9
Marconi, A., Moorwood, A. F. M., Salvati, M., & Oliva, E. 1994, A&A, in press
Mazzarella, J. M., Voit, G. M., Soifer, B. T., Matthews, K., Graham, J. R., Armus, L., & Shupe, D. 1994, AJ, 107, 1274
Mountain, C. M., Robertson, D. J., Lee, T. J., & Wade, R. 1990, Proc. SPIE, 1235, 25
Perault, M. 1987, Ph.D. thesis, Univ. of Paris
Planesas, P., Mirabel, I. F., & Sanders, D. B. 1991, ApJ, 370, 172
Press, W. H., Teukolsky, S. A., Vetterling, W. T., & Flannery, B. P. 1992, Numerical Recipes in FORTRAN: The Art of Scientific Computing (Cambrdige: Cambridge Univ. Press)
Ridgway, S. E., Wynn-Williams, C. G., & Becklin, E. E. 1994, ApJ, 428, 609
Rotaciuc, V., Krabbe, A., Cameron, M., Drapatz, S., Genzel, R., Sternberg, A., & Storey, J. W. V. 1991, ApJ, 370, L23
Sanders, D., Egami, E., Mirabel, I., Lipari, S., & Soifer, B. 1994, AJ, submitted
Sanders, D. B., Scoville, N. Z., & Soifer, B. T. 1991, ApJ, 370, 158
Sanders, D. B., Soifer, B. T., Elias, J. H., Madore, B. F., Matthews, K., Neugebauer, G., & Scoville, N. Z. 1988a, ApJ, 325, 74
Sanders, D. B., Soifer, B. T., Elias, J. H., Neugebauer, G., & Matthews, K. 1988b, ApJ, 328, L35
Scoville, N. Z., Sargent, A. I., Sanders, D. B., & Soifer, B. T. 1991, ApJ, 366, L5
Soifer, B. T., et al. 1987, ApJ, 320, 238
Veilleux, S., Kim, D. C., Sanders, D. B., Mazzarella, J. M., & Soifer, B. T. 1994, ApJ, submitted